IEEE Access
Multidisciplinary | Rapid Review | Open Access Journal

Received December 6, 2021, accepted December 22, 2021, date of publication December 23, 2021,
date of current version January 27, 2022.

Digital Object Identifier 10.1109/ACCESS.2021.3138147

Realize Load-Independent Output With Soft Switching Based on Switched Capacitor for Wireless Charger System

BING CHENG AND LIANGZONG HE
Electrical Engineering Department, Xiamen University, Xiamen 361012, China

Corresponding author: Liangzong He (hlz190213@163.com)

This work was supported in part by the National Natural Science Foundation Project under Grant 62071406, and in part by the Natural Science Foundation of Guangdong Province General Project under Grant 2021A1515011710.

ABSTRACT Wireless power transfer (WPT) technology has been given more and more attentions in lithium-ion batteries charging. To ensure the charging reliability and improve the charging efficiency, the load-independent current and voltage output with inductive input impedance to realize zero voltage switching (ZVS) condition are usually necessary in WPT system. However, too many power switches and passive components in the existing methods bring the whole system inefficient, bulky and uneconomical. In this paper, the switched-controlled-capacitance (SCC) structure is investigated. Then a hybrid topology, where the SCC is employed to adjust the secondary resonant capacitor, is proposed to achieve the desired load-independent current and voltage output under two different operation frequencies. Simultaneously, the soft switching of all power devices can also be realized during the whole charging period. Besides, the transformation between two operation modes by SSC and operation frequency adjustment is very convenient and smooth, which enhances the switching safety. Finally, an experimental prototype with 60V and 3A is built to validate the proposed wireless battery charger system.

INDEX TERMS Wireless power transfer (WPT), constant current (CC), constant voltage (CV), zero voltage switching (ZVS), switched-controlled-capacitance (SCC).

I. INTRODUCTION

Wireless power transfer (WPT) technology, which can realize the transmission of electric energy from the power side to the load side through magnetic field without twisted electrical wires, has the advantages of convenience, safety, high flexibility and strong environmental adaptability. With the launch of a lot of related work, this technology has gradually made great progress in transmission distance, conversion efficiency, security, etc. Furthermore, it has been widely applied to various applications, including low-power biomedical implants [1], [2], consumer electronics [3], [4], equipment in harsh environment [5], [6], high-power electric vehicles (EV) [7], [8] and other industrial areas.

Among the above applications, batteries are usually used as energy storage units. In order to prolong the service life of battery, the battery charging mode is important. The typical charging profile for Li-ion batteries includes a constant current (CC) charging mode and a constant voltage (CV) charging mode [9]. At the beginning, the CC charging mode with the preset charging current I_B is executed. Simultaneously, the battery voltage rises quickly to preset charging voltage V_B, and then the charging mode turns into CV mode with the constant output voltage VB immediately. In CV mode, the charging current drops exponentially. Finally, the charging process is terminated until the charging current is equal to the one-tenth of preset charge current [10]. In addition, it is clearly that the equivalent resistance of the battery R_B (calculated by the output current and voltage) changes considerably during the charging process. As a result, the load-independent CC and CV charging characteristics with ZVS conditions are significant for WPT systems for batteries charging.

To obtain the required constant output current or voltage efficiently, a lot of studies on control methodologies have been carried out. Even the variation range of mutual inductance is very wide, the proposed converter can obtain a

The associate editor coordinating the review of this manuscript and approving it for publication was Chi-Seng Lam.

stable charging voltage by regulating the operation frequency to be a proper value rapidly. Moreover, the power factor and efficiency can be adjusted during the charging process as well [11], however, due to the existence of frequency splitting, wide range of frequency variation corresponding with the wide range of load change is unacceptable, which will affect the reliability and stability of whole WPT system [12]. In order to reduce the range of frequency regulation, an implementation method of the three-loop control strategy is proposed, then the system can operate at a demanded condition, including the preset input impedance angle and the required voltage output, by adjusting the frequency and phase shift angle [13], nevertheless, the frequency-duty-cycle hybrid adjustment makes the implementation of control process more complicated. An additional BUCK-BOOST converter is added in the transmitter side or receiving side to realize the constant charging current or the charging voltage [14]. However, too many components used on the DC-DC converter will increase the system size and the device cost. Other common shortcomings including too many variables to be measured. By comparison, the realization of load-independent constant output by compensation network structure not only saves space and cost, but also avoids complex control circuits [15], [16].

According to the typical charging curve, the CC mode should be smoothly changed to the CV mode when the output voltage increases to preset charging voltage. An enormous amount of researches based on various control methods have been done in the last decades for WPT systems. And these methods can be simply divided into two catenaries: 1) multiple additional switches; 2) two different operating frequencies. Firstly, multiple switches on the receiver side or transmission side are used to reconfigure the compensation network structure in order to select the CC mode or CV mode [17]–[22]. However, it needs multiple power switches and extra passive components on the compensation network part, which will increase the cost and installation space. In order to avoid the use of additional switches, a complex theoretical analysis to realize load-independent CC and CV charging without additional power switches at two different switching frequencies are given for the WPT system [23]–[25]. However, too many components used on the compensation network part still make the system bulky. To address above issues, the paper systematically analyzes the load-independent output and input impedance characteristics of the simple SS compensation topology. Then, an optimal hybrid topology, combining SS compensation topology with SCC, is proposed, which reduces the numbers of passive components. Therefore, the system size and cost greatly reduces. Besides, due to the implementation of SCC structure, the load-independent voltage and current output characteristics and soft switching can be maintained when the coils misalignment happens. In addition, the transformation between two operation modes by SSC and operation frequency adjustment is very convenient and smooth, which enhances the switching safety.

The paper is organized as follows. The proposed SCC structure and its operation principle are introduced in Section II. Simultaneously, a hybrid WPT topology is proposed based on proposed SCC structure. Then in Section III, the output and input characteristics of proposed hybrid WPT system are analyzed. The Section IV is the corresponding control strategy. Finally, a WPT charger platform with 3-A charging current and 60-V charging voltage is built to test the above analysis in Section V. Then follows the conclusion in Section VI.

II. WPT SYSTEM WITH SCC

A. SCC

The SCC technology was first introduced in [26] and it had been used in many resonant converters to obtain required circuit performance, such as soft switching under coils misalignment [27], [28], constant power output [29] and so on. The operation principle of SCC is analyzed in this section and the relationship between the equivalent capacitance of SCC and the conduction duty cycle is derived.

Fig. 1(a) shows the SCC employed in this paper. The SCC consists of a switch S, a capacitor C_a and an additional capacitor C_b. The equivalent capacitance value can be regulated by changing the turn-on duty cycle of S.

Some typical waveforms in the SCC part are depicted in Fig.1(b). Assuming the input current i_x is sinusoidal, for the positive part of i_x, the S is turned on at the zero-crossing point

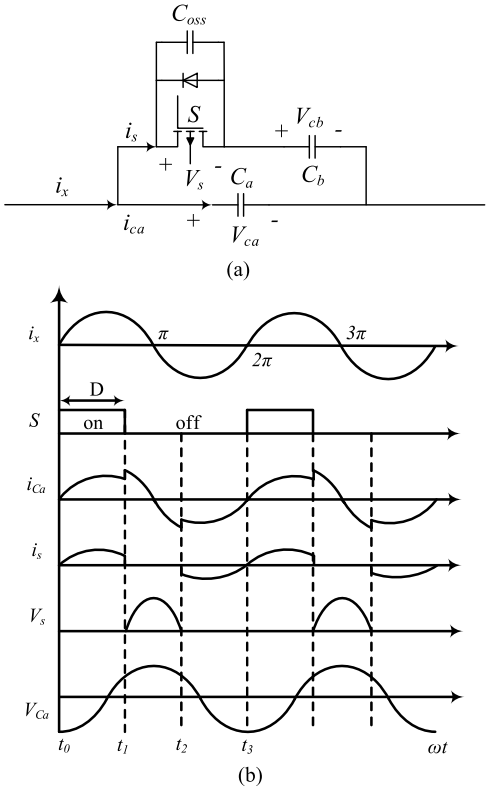

FIGURE 1. SCC. (a) Used SCC structure. (b) Typical waveforms for SCC.

of i_x, then the i_x charges the C_a and C_b simultaneously, the i_x will be divided into i_s and i_{Ca} according to the value of C_a and C_b. When the S is turned off under zero voltage at t_1, the i_x flows only via the C_a and the voltage V_{Ca} across the C_a continues to rise until π. For the negative half cycle of i_x from π to 2π, the i_x only discharges C_a first until t_3, by now the instantaneous value of V_{Ca} will be equal to the V_{Cb}, therefore, the C_a and C_b are both discharged by i_x, it is noted that the current discharges C_b via the antiparallel diode of S. It is noting that the soft switching of S is realized during the whole operation process.

The expression of the equivalent capacitance C_{sc} and D yields according to [29].

$$C_{sc} = \frac{2DC_aC_b}{C_a + C_b(1-2D)} + C_a \tag{1}$$

where $0 \le D \le 0.5$.

Furthermore, the capacitance ratio of C_{sc}/C_a against the turn-on duty cycle D is shown in Fig. 2 according to the equation (1). In Fig.2, there are two important operation points to be introduced in detail. When S is turned off in the whole period, C_b does not affect the operation of C_a again and C_{sc} is equal to C_a. On the contrary, when the D is larger than 0.5, which means the S is always on, the C_a and C_b are in parallel connection during the operation process. Therefore, the C_{sc} is the summation of C_a and C_b and could not be regulated again. When the D changes from 0 to 0.5, the value of C_{sc} changes rapidly with the increasing of D. In theory, the equivalent capacitance can be regulated from $C_a + C_b$ to C_a. It is noted that the equivalent capacitance is only related to D, which greatly increases the robustness of proposed SCC structure.

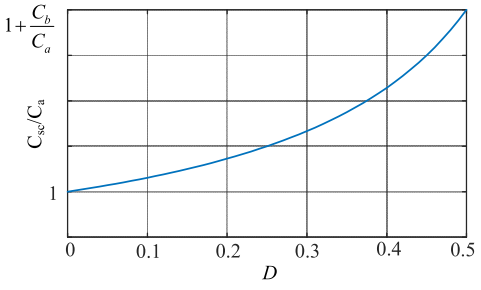

FIGURE 2. The capacitance ratio of C_{sc}/C_a against duty cycle D.

As for the parallel capacitor C_{oss} of switch S, when S is turned on, the C_{oss} is shorted. When S is turned off, the C_{oss} is connected with C_{b} in series and the equivalent capacitor can be calculated as

$$C_{eq1} = \frac{C_{oss}C_b}{C_{oss} + C_b} \tag{2}$$

The power switch with a very small C_{oss} can be chosen as S, for example, C2M0040120D with 47pF C_{oss}. Therefore, the value of C_{eq1} does not exceed 47pF. Then the equivalent capacitor C_{sc} of SCC structure can be seen as $C_a + C_{eq1}$. Normally, the value of C_a is about dozens nF, as a result, the switch capacitance C_{oss} can be ignored when S is turned off. In summary, the parallel capacitor C_{oss} of switch S can be ignored during the normal operation of SCC as long as the S is chosen properly.

B. PROPOSED WPT SYSTEM WITH SCC

The proposed WPT system with SCC is shown in Fig. 3(a). The resonant tank in the primary side consists of a transferring coil L_p and its corresponding compensation capacitor C_p. The SCC is used as the compensation capacitor of receiving coil L_s. The equivalent circuit based on the mutual inductance theory is shown in Fig. 3(b). And L_m is the magnetizing inductance referred to the primary side, which usually represents the energy transferred to the secondary side.

$$k = \frac{L_m}{\sqrt{L_pL_s}} \tag{3}$$

where k is the coupling coefficient, which is determined by the horizontal and vertical offsets of coupling coils. It is noting that the mutual L_{m} should be smaller than the self-inductance of the primary and secondary side coils.

C. ANALYSIS OF LOAD-INDEPENDENT OUTPUT AND INPUT IMPEDANCE CHARACTERISTICS IN CC MODE

The transmission characteristics of proposed WPT system with SCC structure is analyzed to obtain the desired C_{sc} value for CC/CV output. Based on the Kirchhoff Voltage Law (KVL), the mathematical expression of the proposed WPT system can be given as

$$\begin{cases} v_p = jX_1i_1 - j\omega_{cc}L_mi_o \\ 0 = (jX_2 + R_{eq})i_o - j\omega_{cc}L_mi_1 \end{cases} \tag{4}$$

where, ω_{cc} indicates the operating angular frequency in CC mode, L_m is the magnetizing inductance referred to the primary side, jX_1 and jX_2 is the equivalent impedances of the corresponding circuit branch. And the related expression can be obtained as

$$\begin{cases} X_1 = \omega_{cc}L_p - \dfrac{1}{\omega_{cc}C_p} \\ X_2 = \omega_{cc}L_s - \dfrac{1}{\omega_{cc}C_{sc1}} \end{cases} \tag{5}$$

With the condition as follows

$$X_1 = 0 \tag{6}$$

The output current is load-independent and the condition for CC output will not be affected by L_m. The corresponding Ac transfer ratio G_{cv} yields in the equation (7). Therefore, if the input voltage is fixed, the output current will be determined by the operating angular frequency ω_{cc} and L_m.

$$G_{cv} = \frac{v_p}{i_o} = -j\omega_{cc}L_m \tag{7}$$

Simultaneously, the input impedance is simplified with the condition (6) as

$$Z_{in} = \frac{\omega_{cc}^2L_m^2(R_{eq} - jX_2)}{R_{eq}^2 + X_2^2} \tag{8}$$

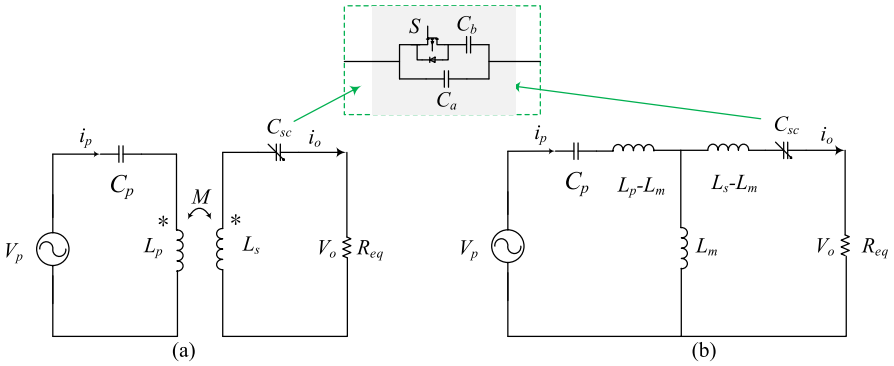

FIGURE 3. Proposed WPT system with SCC (a) Proposed topology. (b) Equivalent circuit based on mutual inductance theory.

And the input impedance angle can be calculated as

$$a_c = a\tan(\frac{|X_2|}{R_{eq}}) \tag{9}$$

In summary, the proposed WPT system can realize load-independent current output with the condition (6). It is notable that the input impedance Z_{in} should be inductive in order to achieve ZVS turn-on for the primary inverter [30]. However, the ZPA means zero phase shift between the input voltage and current, resulting in Z_{in} of purely resistive. Therefore, ZVS and ZPA can never be realized simultaneously. As a result, the realization of ZVS and nearly ZPA becomes the practical choice to improve the system performance. In addition, the turn-off power loss is relatively small due to the existence of C_{oss} (the output capacitor of power MOSFETs), which can be ignored in practical application [31].

D. ANALYSIS OF LOAD-INDEPENDENT OUTPUT AND INPUT IMPEDANCE CHARACTERISTICS IN CV MODE

Similar to the analysis process at CC mode, the KVL equation can be changed into (10), which is shown as follows

$$\begin{cases} v_p = jX_1 i_1 - j\omega_{cv} L_m i_o \\ v_o = j\omega_{cv} L_m i_1 - jX_2 i_o \end{cases} \tag{10}$$

where X_1 and X_2 is defined as

$$\begin{cases} X_1 = \omega_{cv} L_p - \dfrac{1}{\omega_{cv} C_p} \\ X_2 = \omega_{cv} L_s - \dfrac{1}{\omega_{cv} C_{sc2}} \end{cases} \tag{11}$$

To obtain load-independent CV output, follow condition should be satisfied as

$$X_1 X_2 = \omega_{cv}^2 L_m^2 \tag{12}$$

Then the voltage transformation ratio can be expressed as

$$G_{vv} = \frac{v_p}{v_o} = \frac{X_2}{\omega_{cv} L_m} \tag{13}$$

From (11) and (12), the load-independent voltage output can be realized as long as the C_{sc2} is regulated to satisfy the equation (12). Moreover, the load-independent voltage output characteristics will not lose even the L_m varies. Meanwhile, the input impedance can also be given as.

$$Z_{in} = \frac{X_1(X_2 R_{eq} + jR_{eq}^2)}{R_{eq}^2 + X_2^2} \tag{14}$$

And the input impedance angle can be calculated as

$$a_v = a\tan(\frac{R_{eq}}{|X_2|}) \tag{15}$$

According to the (11) and (15), by designing the parameter properly, the input impedance angle is positive, which means the ZVS turn-on can be guaranteed.

According to the above analysis, it can be concluded that the proposed WPT system can achieve load-independent CC and CV outputs with different C_{sc} value and operation frequencies. Moreover, the ZVS condition can also be satisfied both at CC mode and CV mode, which means that the proposed WPT system is the simplest topology to realize load-independent CC/CV with ZVS.

III. EVALUATIONS

From the above analysis, the load-independent CC output and CV output can be realized with an identical set of resonant parameters at two different operation frequencies, respectively. However, the load-independent ZVS condition cannot be achieved in CC and CV mode simultaneously. To solve this problem, an SCC is employed to change the value of secondary resonant capacitor C_{sc}. The proposed hybrid topology with an extra reconfiguration switch is proposed,

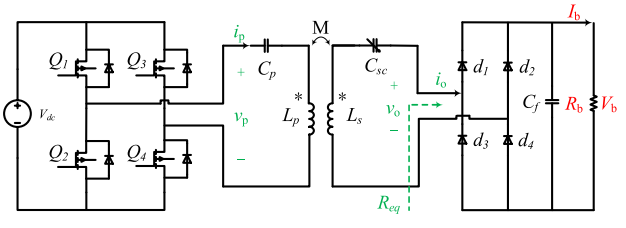

FIGURE 4. The proposed hybrid WPT system with SSC for battery charging.

as shown in Fig. 4. The proposed hybrid topology consists of an dc voltage source V_{dc}, a full-bridge high frequency inverter (HFI) composed of four power switches (Q_1-Q_4), the resonant tank made up of a transmitting coil L_p in the primary side, a receiver coil L_s in the secondary side, and their corresponding series compensation capacitances, a full-bridge rectifier constituted by four diodes (d_1-d_4), the filter capacitance C_f, and the battery load R_b. v_p *and* i_p are the phasor forms of input voltage and current of the compensation network, respectively. V_b and I_b are the preset charging voltage and current obtained from the datasheet of Li-battery. The equivalent series resistances (ESRs) of the resonant inductors and capacitors are assumed to be zero for the convenience of theoretical analysis.

A. PARAMETER DESIGN

As mentioned in above analysis, to realize the load-independent output, special parameters for CC/CV operation condition should be satisfied if the compensation topology has been confirmed. The HFI generates a square voltage with the operation frequency. In order to simplify the parameter design process of the proposed WPT system, the fundamental harmonic approximation (FHA) is adopted and the influence comes from other high-order harmonics are ignored. Then the relationship between the dc input voltage V_{dc} and ac output voltage v_p with the HFI of $D = 0.5$ is given as:

$$v_p = \frac{2\sqrt{2}V_{dc}}{\pi} \tag{16}$$

Besides, the relationship between ac input parameters and dc output parameters of the full-bridge diode rectifier can be given by:

$$\begin{cases} v_o = \dfrac{2\sqrt{2}V_b}{\pi} \\ i_o = \dfrac{\pi\sqrt{2}I_b}{4} \end{cases} \tag{17}$$

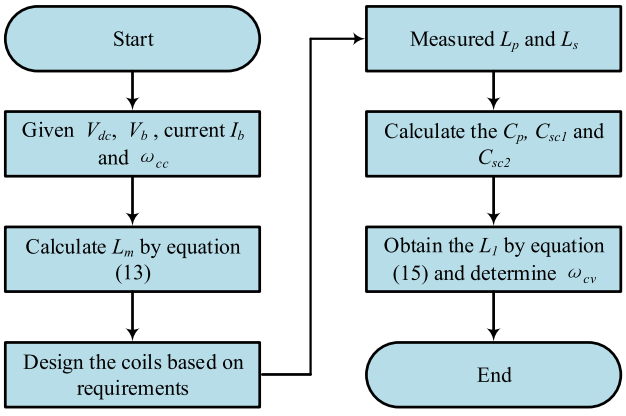

FIGURE 5. Design procedure of the compensation components in the proposed hybrid WPT system.

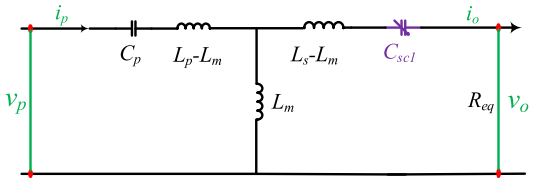

FIGURE 6. The simplified equivalent circuit of the proposed hybrid resonant network circuit for load-independent CC output analysis.

And the equivalent resistor seen from the input end of the full-bridge diode rectifier can be calculated as:

$$R_{eq} = \frac{8R_b}{\pi^2} \tag{18}$$

The parameters are calculated based on the design procedures in Fig. 5. It is noted that the S should be turned on when the whole system works in load-independent CV mode, conversely, in load-independent CC mode, the S should be turned off to change the C_{sc} value.

Based on the above analysis of the proposed matching networks, to achieve the load-independent CC output, the equivalent circuit is simplified to the Fig. 6, and the equivalent variables in Fig. 6 should meet the following resonant condition:

$$\omega_{cc}^2 = \frac{1}{L_p C_p} \tag{19}$$

Then from (7), the magnetizing inductance L_m is determined by the preset charging current i_o, input voltage v_p and load-independent CC operation angle frequency ω_{cc}. And it is given by:

$$L_m = \frac{v_p}{\omega_{cc} i_o} \tag{20}$$

Furthermore, inductive input impedance is required to achieve ZVS condition in the proposed topology, besides, a smaller input impedance angle means a stronger power transfer capability. Thus, the secondary compensation capacitance C_{sc1} should satisfy follow condition

$$\omega_{cc} L_s - \frac{1}{\omega_{cc} C_{sc1}} < 0 \tag{21}$$

Similarly, at CV mode, the equivalent circuit of proposed hybrid WPT system is shown in Fig. 7. Since the values of C_p, L_m, and V_b have been determined in the load-independent CC mode, the operation frequency ω_{cv} for load-independent CV

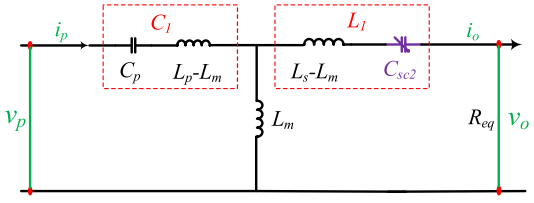

FIGURE 7. The simplified equivalent circuit of the proposed hybrid resonant network circuit for load-independent CV output analysis.

mode and the capacitance C_{sc2} to realize load-independent ZVS condition are derived.

Based on the analysis result in Section II, the equivalent inductance L_1 in the receiving side is decided by the input voltage v_p, output voltage v_o and the magnetizing inductance L_m, and it is given by:

$$L_1 = \frac{L_m(v_o - v_p)}{v_p} \tag{22}$$

Then, according to the parameter resonant condition (11), the operation frequency ω_{cv} for load-independent CV mode is explicated as

$$\omega_{cv}^2 = \frac{(L_1 + L_m)}{\left(C_p L_1 L_m + C_p(L_s - L_m)(L_1 + L_m)\right)} \tag{23}$$

As shown in Fig. 7, the equivalent inductance L_1 consists of three parts, including the inductance L_s-L_m and the secondary series compensation capacitance C_{sc2} Since the operation frequency ω_{cv}, L_s, L_m and L_1 are all given, the value of ZVS compensation capacitance C_{sc2} is then calculated as follow

$$C_{sc2} = 1/\left(\omega_{cv}^2(L_s - L_1 - L_m)\right) \tag{24}$$

B. VERIFICATION OF THE PROPOSED SYSTEM FOR THE LOAD-INDEPENDENT CC/CV CHARGING

It is crucial to test the load-independent and input impedance characteristics for the proposed reconfigurable charging WPT system. Based on the system design parameters in Table 1, the curves of the voltage gain ratio G_{vv} (the ratio of output voltage to input voltage) and the phase angle of the related input impedance Z_{in} as a function of the switching frequency at different equivalent loads are drawn as shown in Fig. 8(a) and (b), respectively. As shown in Fig. 8(a), there are two frequency points (128.58 kHz and 167.49 kHz) that enable the WPT system to keep the ac voltage gain ratio G_{vv} unchanged against load. However, the input impedance angle is negative at the operating frequency point (128.58 kHz), meaning the ZVS condition of primary inverter will not be satisfied at this frequency point (128.58 kHz). Therefore, the frequency point (167.49 kHz) is selected as the operation frequency in CV mode. Moreover, the calculation results of the current transfer ratio G_{cv} (the ratio of input voltage to output current), and input impedance phase angle of the proposed compensation network versus switching frequency at the different load conditions are illustrated in Fig. 9. Seen from Fig. 9, the constant current output with ZVS condition at different loads is satisfied at the same frequency point (150 kHz). The calculation results in Fig. 8 and Fig. 9 show that the hybrid system can realize the desired load-independent CC and CV charging characteristics at two fixed switching frequency points as well as the associated ZVS operation with used SCC structure, respectively.

IV. CONTROL AND DISCUSSION FOR THE CC/CV CHARGING MODES

According to the analysis results in Section III-part A, the load-independent CC output is realized when the switching

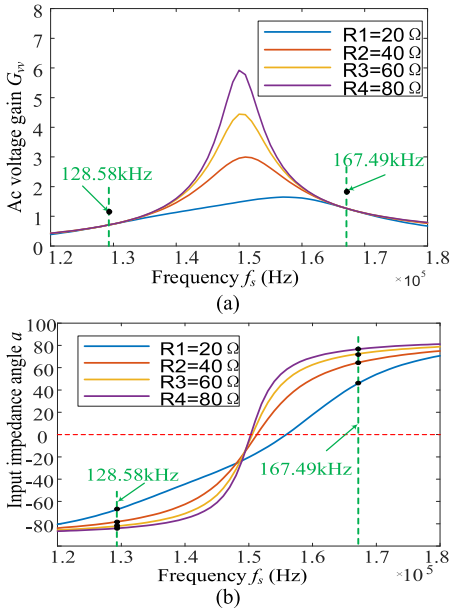

FIGURE 8. Ac voltage gain G_{vv} and phase angle a of Z_{in} against operation frequency f_s in the proposed hybrid WPT system for CV output. (a) G_{vv}. (b) a.

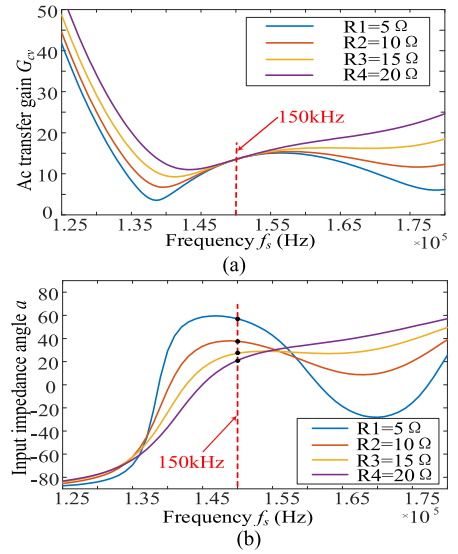

FIGURE 9. Ac transfer gain G_{cv} and phase angle a of Z_{in} against operation frequency f_s in the proposed hybrid WPT system for CC output. (a) G_{cv}. (b) a.

frequency is set at f_{cc}, moreover, the ZVS of front HFI is obtained by controlling the SCC as C_{sc1}. As for the load-independent CV output, the operation frequency should work at the frequency point f_{cv} to achieve load-independent CV output, and the SCC is controlled as C_{sc2} to realize ZVS of the front HFI. In addition, since the resonant currents are bidirectional, it is noted that SiC power MOSFET is employed as the switch S due to its small parasitic capacitance.

Based on the analysis above, the control chart of proposed hybrid WPT system is shown in Fig. 10. At the beginning of charging process, the whole system works at CC mode with

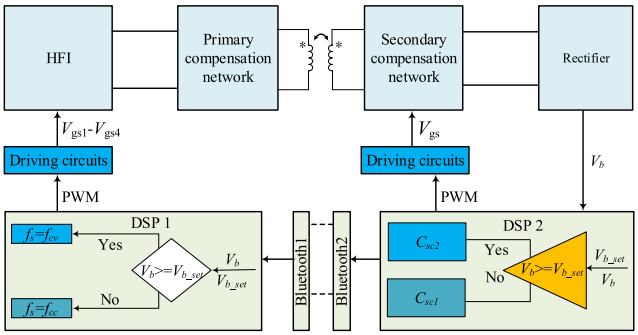

FIGURE 10. The control chart of proposed hybrid WPT system.

the operation frequency f_{cc}, and the SCC is adjusted as C_{sc1}. Since the battery can be modeled as a resistor R_b and its value increases nonlinearly with the charging process according to the battery charging profile, the output voltage will increase in the CC mode. Once the charging voltage V_b hits the predetermined voltage level, the whole system enters into CV mode by switching the operation frequency from f_{cc} to f_{cv}. Simultaneously, the S is given another PWM signal. To avoid the switch current spike caused by the voltage difference across the switch S when the switch is turned on suddenly, a zero crossing comparator can be added to ensure that the switch S is turned on at the time when the secondary resonant current i_{Cs} closes to zero. Therefore, the zero current turn-on of switch S can be realized. Besides, the communication between the primary and secondary circuits can be implemented over Bluetooth to realize a real contactless charging.

When the coupling coefficients varies due to the coils misalignment, the performance of whole system can be introduced as follows.

For the CC mode, if the coupling coefficient varies, the load-independent current output characteristic and soft switching will not be affected, however, the output current value will change at a negative trend.

For the CV mode, the whole system will lose its load-independent voltage output characteristics soft switching, however, the load-independent voltage output characteristic and soft switching can be realized again by changing the equivalent capacitor value of SCC structure. Similarly, the output voltage value will change as well. The output current value in CC mode and voltage value in CV mode can be regulated by adding a DC/DC converter.

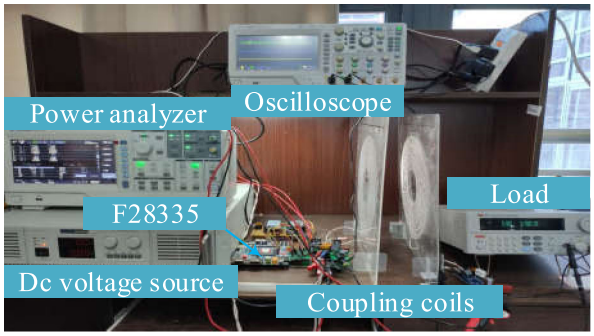

FIGURE 11. Laboratory setup of the proposed hybrid WPT system.

V. CONTROL AND DISCUSSION FOR THE CC/CV CHARGING MODES

A. EXPERIMENTAL PLATFORM

To verify the above analysis, an experimental prototype for contactless battery charger with 3-A charging current and 60-V charging voltage has been constructed as is shown in Fig. 11 and the parameters are listed in Table 1. The semiconductor switching devices MOSFET (C2M0080120D) is chosen to form the HFI due to its lower on-resistance and good performance in high frequency environment. The CC operation frequency f_{cc} and CV operation frequency f_{cv} is set as 150 kHz and 167.49 kHz, respectively. Polypropylene film capacitances are selected for the resonant capacitance in the compensation network part. To keep the error between the measured and designed capacitance value as small as possible and decrease the parasitic resistance value of the capacitance bank, the resonant capacitor is designed by connecting multiple standard capacitances in parallel. Schottky diodes PSM20U200GS with $V_F = 0.95$V at rated power are used at the receiving side full-bridge uncontrolled rectifier. The rectifier with capacitive output filter is adopted to rectify the ac output of the compensation topology before connecting to the battery load. As for the control circuits, the DSP (TMS320F28335) control unit is adopted to generate the driving signals required for the switching devices in the transmitting side.

Planar spiral coil is chosen as the transmitting and receiving coils of this proposed WPT system due to its strong coupling coefficient and small size. Simultaneously, to keep

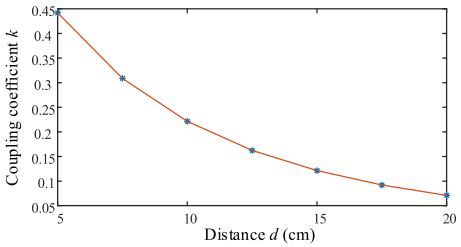

FIGURE 12. The coupling coefficient k against the coils distance d.

TABLE 1. Parameters for the proposed hybrid WPT system.

Parameter	Designed value	Measured value
Self-inductance L_p	50.25uH	57.84uH
Self-inductance L_s	50.25uH	58.04uH
Resonant capacitance C_p	19.277nF	19.378nF
Resonant capacitance C_{s1}	15nF	14.952nF
Resonant capacitance C_{s2}	22.559nF	22.421nF
Distance d	10cm	10cm
Self-resistances R_p/R_s	0.124/0.129 Ω	0.124/0.129 Ω
Coupling coefficient k	0.2454	0.2454
Output parameter V_b/I_b	60V/3A	60V/3A

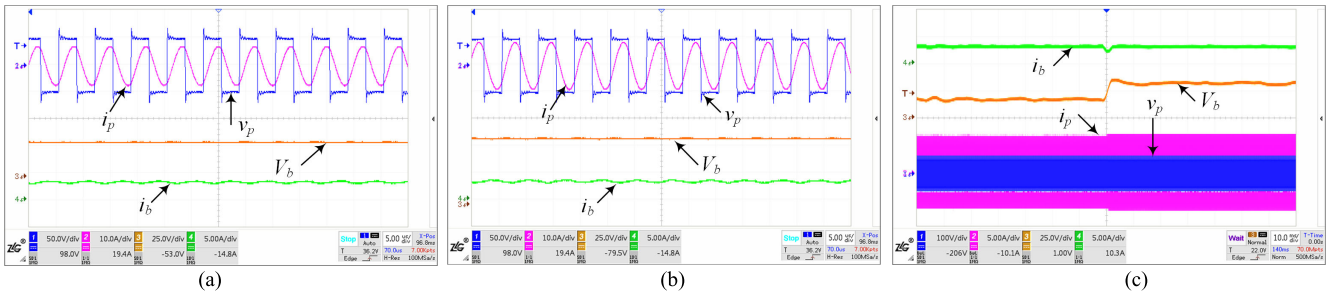

FIGURE 13. Experimental waveforms of v_p, i_p, V_b, and i_b at CC mode. (a) $R_b = 10\ \Omega$. (b) $R_b = 20\ \Omega$. (c) Load step changes from 5Ω to 10Ω.

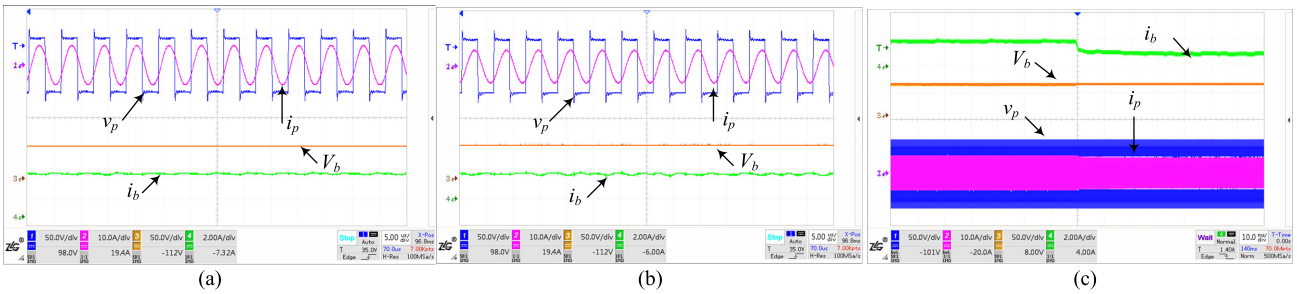

FIGURE 14. Experimental waveforms of v_p, i_p, V_b, and i_b at CV mode (a) $R_b = 20\ \Omega$, (b) $R_b = 40\ \Omega$. (c) Load step changes from 30Ω to 60 Ω.

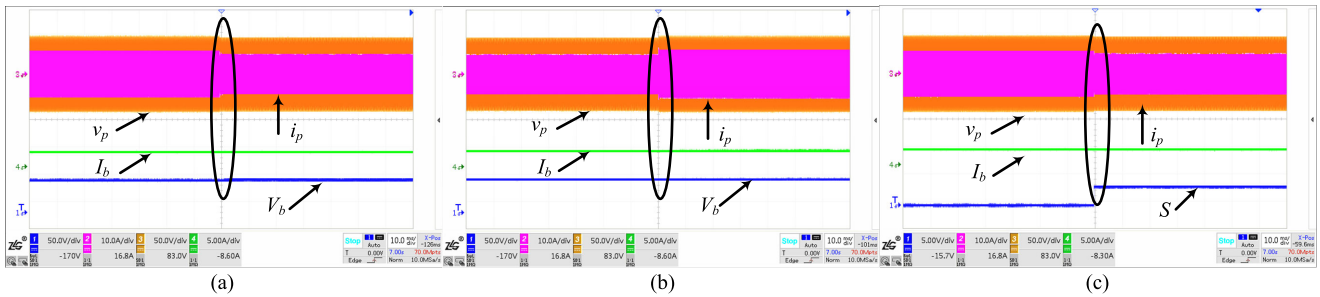

FIGURE 15. Experimental waveforms of v_p, i_p, V_b, and i_b (a) CC to CV. (b) CV to CC. (c) The driving signal from CC to CV.

the consistency of parameters and achieve resonance conveniently, the transmitting and the receiving coil are designed of the same specification. Besides, a larger wire diameter means more obvious skin effect and larger equivalent series resistance, therefore, the Litz wire (350 strands and diameter of 2.5mm) is adopted for coupling coils design in the paper. Fig. 12 shows the measured coupling coefficient k against the distance between the transferring and receiving side, which can be used as a reference standard in the parameter design process.

B. EXPERIMENTAL RESULTS

Since the charging process starts in CC mode, the load-independent CC output mode under a constant dc voltage (50V in the paper) at different loads is discussed firstly. In Fig. 13, the waveforms of the modulated voltage v_p, input current i_p, output current i_b and output voltage V_b at two different loads 10 Ω and 20 Ω are collected. And it is obviously seen that the charging current i_b is kept at the desired 3A with operation frequency 150 KHz. The dynamic performance for the proposed WPT system with a load variation are analyzed, and the transient experimental waveforms is given in Fig. 13(c). In Fig. 13(c), the WPT system still operates at 150 kHz, the output current can maintain 3.0A with a slight fluctuation when the output load changes from 5 Ω to 10 Ω, simultaneously, the output charging voltage V_b varies from 15.06V to 30.23V. Apparently, this proposed hybrid WPT system can achieve load-independent CC output if the parameters are well-designed. In addition, according to the input impedance analysis, the equivalent value of C_{sc} is chosen as 15nF to achieve ZVS by adjusting S conduction duty cycle properly. In Fig. 13(a) and Fig. 13(b), the input current lags behind the input voltage, therefore, the V_{ds} is choked to nearly zero when the V_{gs} is given. In summary, the load-independent CC output with ZVS turn-on is well achieved in the proposed WPT system.

TABLE 2. Comparison with different papers for load-independent CC and CV outputs with ZVS condition.

	Coils	Resonant capacitance	Resonant inductor	Additional switches	Measured parameters	Switching safety	ZVS	Efficiency	Output Value
[17]	4	4	0	2	V_B	No	√	92.25%	48V/3.6A
[18]	3	5	1	2	none	No	ZPA	90.8%	96V/4A
[19]	2	2	1	3	i_{Bat}, V_{Bat}	No	√	93%	15V/1A
[22]	2	4	1	2	V_B	No	√	92.81%	96V/2A
[23]	3	3	0	0	U_B, I_B	Yes	√	93.8%	56V/4.6A
Proposed	2	3	0	1	V_b,i_{Cs}	Yes	√	91.51%	60V/3A

Where the "none" means that the measured parameters are not given in the paper and "√"means that the ZVS condition is satisfied.

The output mode will turn into CV mode rapidly when the output charging voltage increases to 60V. The main waveforms including the modulated voltage v_p, input current i_p, output current i_b and output voltage V_b at two different loads 20 Ω and 40 Ω are given in Fig. 14. Obviously, the charging voltage V_b can be kept at about 60 V in the CV operation frequency 167.7 KHz. Similarly, the robust performance of the hybrid WPT system in CV mode are tested in Fig. 14(c) when load varies. The charging voltage can maintain 60 V with a small fluctuation when the output load is changed from 30 Ω to 60 Ω, simultaneously, the output charging current i_b decreases from 1.943 A to 0.9869 A. Generally, the load-independent output characteristic performs well in the proposed hybrid WPT system. Besides, to realize ZVS condition, the S is controlled and the equivalent value of C_{sc} is 22.367nF. As is shown in Fig. 14(a) and Fig. 14(b), the input current lags behind the input voltage as well. Therefore, the ZVS turn-on in load-independent CV mode is also realized in the proposed WPT system. Furthermore, the ZVS condition is satisfied during the full charging process. It is noted that the ZVS turn-off is not fully achieved due to relatively small drain-source parasitic capacitance, however, the turn-off power loss is relatively small, which can be ignored in practical application.

The mode transfer performance is validated in Fig. 15. As the transient waveforms of mode switching from CC to CV mode in Fig. 15(a), the charging voltage and current almost has no fluctuation during the switching process. Apparently, there is no voltage and current spike during the transformation. The corresponding driving signal for switch S is shown in Fig. 15(c). Similarly, the CC mode can be transferred smoothly from the CV mode. In short, the switching process of proposed system is more fluent and acceptable.

The whole charging profile with the charging voltage and current against lg(R_b) is shown in Fig. 16(a). Obviously, the experimental data meets well with the required charging profile. To further evaluate the transfer performance of the proposed hybrid WPT system, the power analyzer PA2000mini is used to measure the overall DC-DC transmission efficiency. The charging efficiency curve (from the dc voltage source to the battery load) of the hybrid WPT system versus lg(R_b) during the entire charging process is measured and is shown in Fig. 16(b). The efficiency rises from 80.8% to the peak point of 90.38% with the increasing of R_b in CC mode and then

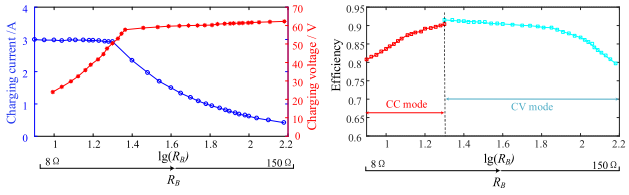

(a) (b)

FIGURE 16. Experimental results. (a) Measured charging profile. (b) Measured efficiency curve.

drops back 80.3% from 91.51% in CV charging mode. It is noted that the minimum charging efficiency is 80.3% when R_b is 150Ω, which is suitable for battery wireless charging applications. Besides, the transmission efficiency difference at the crossing point of two modes is caused by the different resonant network in the CV and CC mode.

In this paper, the equivalent capacitor value of SCC structure changes once from C_{sc1} in CC mode to C_{sc2} in CV mode. The another advantage of proposed SCC structure is the maintain of load-independent output characteristic at different L_m conditions. As is shown in Fig. 17, with the increasing of L_m, the required C_{sc2} to realize the load-independent CV output under fixed resonant frequency will increase, furthermore, the turn-on duty cycle D of SCC structure for C_{sc2} is increasing accordingly. Besides, from (7) and (13), the output current value in CC mode and voltage value in CV mode will change due to the variation of L_m, which meets well with the experimental results. However, the output can be regulated by many common methods, such as the phase shift control at the active rectifier, addition of another DC/DC converter and so on.

In order to reflect the superiority in fewer components and easier control method of the proposed two-coil WPT system, comparison about the compensation network part with other papers are listed in Table 2. The high-frequency resonant inductor occupies a high proportion in the volume of system. Therefore, the size of WPT system can be evaluated based on the number of resonant inductors and coils. The cost is dependent on the component counts. And the complexity of feedback circuits is related to the detection variables and corresponding information processing. It can be concluded from the table that the number of passive components and additional switches are both relatively less than [17]–[19] and [22], [23], which means a smaller system size and lower

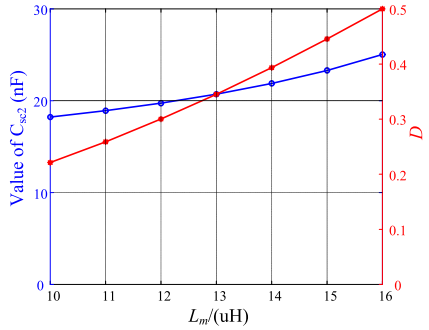

FIGURE 17. The equivalent capacitor C_{sc2} and corresponding D to maintain load-independent output at different L_m conditions.

system cost. And only the output voltage is needed to be measured, moreover, the requirement for control circuit is lower, which makes it easy to implement. Besides, compared with [17], [19] and [22], the addition of zero crossing comparator avoids the switches current spike during the mode switching, which increases the switching safety of proposed system. In other words, the proposed hybrid WPT system is superior to other researches in terms of the component number, system size, system safety and control method for load-independent output with ZVS condition.

VI. CONCLUSION

This article proposes a WPT system with SCC for wireless battery charger. The operation principle of the SCC is introduced and the equivalent capacitor of SCC can be regulated by controlling the turn-on duty cycle of switch. With the assistance of SCC structure, load-independent CC and CV output can be obtained successfully under two operating frequencies. Moreover, ZVS operation can be realized for the primary power switches both at CC and CV modes too. Meanwhile, two operation modes can be transferred smoothly according a wireless communication. Compared with the counterparts, the proposed topology has less components, simpler control strategy and safer transformation process. Finally, an experimental prototype was built and the experimental results agree with the theoretical analysis well with a maximum efficiency up to 91.51%.

REFERENCES

[1] T. D. Dissanayake, A. P. Hu, S. Malpas, L. Bennet, A. Taberner, L. Booth, and D. Budgett, "Experimental study of a TET system for implantable biomedical devices," *IEEE Trans. Biomed. Circuits Syst.*, vol. 3, no. 6, pp. 370–378, Dec. 2009.

[2] H. Liu, Q. Shao, and X. Fang, "Modeling and optimization of class-E amplifier at subnominal condition in a wireless power transfer system for biomedical implants," *IEEE Trans. Biomed. Circuits Syst.*, vol. 11, no. 1, pp. 35–43, Feb. 2017.

[3] Q. Li and Y. C. Liang, "An inductive power transfer system with a high-Q resonant tank for mobile device charging," *IEEE Trans. Power Electron.*, vol. 30, no. 11, pp. 6203–6212, Nov. 2015.

[4] S. Y. R. Hui and W. W. C. Ho, "A new generation of universal contactless battery charging platform for portable consumer electronic equipment," *IEEE Trans. Power Electron.*, vol. 20, no. 3, pp. 620–627, May 2005.

[5] C. Cai, J. Wang, R. Liu, Z. Fang, P. Zhang, M. Long, M. Hu, and Z. Lin, "Resonant wireless charging system design for 110-kV high-voltage transmission line monitoring equipment," *IEEE Trans. Ind. Electron.*, vol. 66, no. 5, pp. 4118–4129, May 2019.

[6] T. Orekan, P. Zhang, and C. Shih, "Analysis, design, and maximum power-efficiency tracking for undersea wireless power transfer," *IEEE J. Emerg. Sel. Topics Power Electron.*, vol. 6, no. 2, pp. 843–854, Jun. 2018.

[7] W. Li, H. Zhao, S. Li, J. Deng, T. Kan, and C. C. Mi, "Integrated LCC compensation topology for wireless charger in electric and plug-in electric vehicles," *IEEE Trans. Ind. Electron.*, vol. 62, no. 7, pp. 4215–4225, Jul. 2015.

[8] S. Moon and G.-W. Moon, "Wireless power transfer system with an asymmetric four-coil resonator for electric vehicle battery chargers," *IEEE Trans. Power Electron.*, vol. 31, no. 10, pp. 6844–6854, Oct. 2016.

[9] A. Khaligh and Z. Li, "Battery, ultracapacitor, fuel cell, and hybrid energy storage systems for electric, hybrid electric, fuel cell, and plug-in hybrid electric vehicles: State of the art," *IEEE Trans. Veh. Technol.*, vol. 59, no. 6, pp. 2806–2814, Jul. 2010.

[10] F. A. V. Pinto, L. H. M. K. Costa, and M. D. de Amorini, "Modeling spare capacity reuse in EV charging stations based on the Li-ion battery profile," in *Proc. Int. Conf. Connected Vehicles Expo (ICCVE)*, Vienna, Austria, Nov. 2014, pp. 92–98.

[11] N. Liu and T. G. Habetler, "Design of a universal inductive charger for multiple electric vehicle models," *IEEE Trans. Power Electron.*, vol. 30, no. 11, pp. 6378–6390, Nov. 2015.

[12] W. Q. Niu, J. X. Chu, W. Gu, and A. D. Shen, "Exact analysis of frequency splitting phenomena of contactless power transfer systems," *IEEE Trans. Circuits Syst. I, Reg. Papers*, vol. 60, no. 6, pp. 1670–1677, Jun. 2013.

[13] Y. Jiang, L. Wang, Y. Wang, J. Liu, M. Wu, and G. Ning, "Analysis, design, and implementation of WPT system for EV's battery charging based on optimal operation frequency range," *IEEE Trans. Power Electron.*, vol. 34, no. 7, pp. 6890–6905, Jul. 2019.

[14] Z. Huang, S.-C. Wong, and C. K. Tse, "Control design for optimizing efficiency in inductive power transfer systems," *IEEE Trans. Power Electron.*, vol. 33, no. 5, pp. 4523–4534, May 2018.

[15] Y. Wang, Y. Yao, X. Liu, and D. Xu, "S/CLC compensation topology analysis and circular coil design for wireless power transfer," *IEEE Trans. Transport. Electrific.*, vol. 3, no. 2, pp. 496–507, Jun. 2017.

[16] W. Zhang and C. C. Mi, "Compensation topologies of high-power wireless power transfer systems," *IEEE Trans. Veh. Technol.*, vol. 65, no. 6, pp. 4768–4778, Jul. 2016.

[17] Y. Li, J. Hu, M. Liu, Y. Chen, K. W. Chan, Z. He, and R. Mai, "Reconfigurable intermediate resonant circuit based WPT system with load-independent constant output current and voltage for charging battery," *IEEE Trans. Power Electron.*, vol. 34, no. 3, pp. 1988–1992, Mar. 2019.

[18] Y. Li, Q. Xu, T. Lin, J. Hu, Z. He, and R. Mai, "Analysis and design of load-independent output current or output voltage of a three-coil wireless power transfer system," *IEEE Trans. Transport. Electrific.*, vol. 4, no. 2, pp. 364–375, Jun. 2018.

[19] X. Qu, H. Han, S.-C. Wong, C. K. Tse, and W. Chen, "Hybrid IPT topologies with constant current or constant voltage output for battery charging applications," *IEEE Trans. Power Electron.*, vol. 30, no. 11, pp. 6329–6337, Nov. 2015.

[20] K. Song, Z. Li, J. Jiang, and C. Zhu, "Constant current/voltage charging operation for series-series and series-parallel compensated wireless power transfer systems employing primary-side controller," *IEEE Trans. Power Electron.*, vol. 33, no. 9, pp. 8065–8080, Sep. 2018.

[21] M. Xingkui, J. Chen, Y. Zhang, and J. Dong, "A simple and reconfigurable wireless power transfer system with constant voltage and constant current charging," *IEEE Trans. Power Electron.*, early access, Oct. 29, 2021, doi: 10.1109/TPEL.2021.3123869.

[22] R. Mai, Y. Chen, Y. Li, Y. Zhang, G. Cao, and Z. He, "Inductive power transfer for massive electric bicycles charging based on hybrid topology switching with a single inverter," *IEEE Trans. Power Electron.*, vol. 32, no. 8, pp. 5897–5906, Aug. 2017.

[23] L. Yang, X. Li, S. Liu, Z. Xu, C. Cai, and P. Guo, "Analysis and design of three-coil structure WPT system with constant output current and voltage for battery charging applications," *IEEE Access*, vol. 7, pp. 87334–87344, 2019.

[24] J. Lu, G. Zhu, D. Lin, S.-C. Wong, and J. Jiang, "Load-independent voltage and current transfer characteristics of high-order resonant network in IPT system," *IEEE J. Emerg. Sel. Topics Power Electron.*, vol. 7, no. 1, pp. 422–436, Mar. 2019.

[25] Z. Huang, S. C. Wong, and C. K. Tse, "Design of a single-stage inductive-power-transfer converter for efficient EV battery charging," *IEEE Trans. Veh. Technol.*, vol. 66, no. 7, pp. 5808–5821, Jul. 2017.

[26] W. J. Gu and K. Harada, "A new method to regulate resonant converters," *IEEE Trans. Power Electron.*, vol. 3, no. 4, pp. 430–439, Oct. 1988.

[27] D.-H. Kim and D. Ahn, "Self-tuning LCC inverter using PWM-controlled switched capacitor for inductive wireless power transfer," *IEEE Trans. Ind. Electron.*, vol. 66, no. 5, pp. 3983–3992, May 2019.
[28] J. Zhang, J. Zhao, Y. Zhang, and F. Deng, "A wireless power transfer system with dual switch-controlled capacitors for efficiency optimization," *IEEE Trans. Power Electron.*, vol. 35, no. 6, pp. 6091–6101, Jun. 2020.
[29] L. He and D. Guo, "An active switched-capacitor half-wave receiver with high efficiency and reduced components in WPT system," *IEEE Trans. Ind. Electron.*, vol. 68, no. 12, pp. 12119–12129, Dec. 2021.
[30] S. Li, W. Li, J. Deng, T. D. Nguyen, and C. C. Mi, "A double-sided LCC compensation network and its tuning method for wireless power transfer," *IEEE Trans. Veh. Technol.*, vol. 64, no. 6, pp. 2261–2273, Jun. 2015.
[31] L. He, X. Xu, J. Chen, J. Sun, D. Guo, and T. Zeng, "A plug-play active resonant soft switching for current-auto-balance interleaved high step-up DC/DC converter," *IEEE Trans. Power Electron.*, vol. 34, no. 8, pp. 7603–7616, Aug. 2019.

BING CHENG was born in Henan, China, in 1996. He received the B.E. degree from Xiamen University, Xiamen, China, in 2018, where he is currently pursuing the Ph.D. degree with the Department of Instrumental and Electrical Engineering. His research interests include wireless power transfer systems, DC/DC conversion topology, and switched controlled capacitor converters.

LIANGZONG HE was born in Hunan, China, in 1984. He received the B.Sc. degree from Jilin University, Changchun, China, in 2006, and the Ph.D. degree from the Huazhong University of Science and Technology, Wuhan, China, in 2012. From November 2009 to August 2011, he was a joint Ph.D. Education Student with Michigan State University, East Lansing, MI, USA. In September 2012, he joined as an Assistant Professor at Xiamen University, Xiamen, China, where he has been a Professor, since August 2019. His research interests include high-efficient power conversion, dc–dc converters, switched-capacitor converters, Z-source converters, wireless power transmission, and battery management systems.